
Article:
Sharma, R., Verth, G. and Erdelyi, R. (2017) Dynamic Behavior of Spicules Inferred from Perpendicular Velocity Components. Astrophysical Journal, 840 (2). ARTN 96. pp. 840-896. ISSN 0004-637X

https://doi.org/10.3847/1538-4357/aa6d57

The Astrophysical Journal, 840:96 (9pp), 2017 May 10 https://doi.org/10.3847/1538-4357/aa6d57

Dynamic Behavior of Spicules Inferred from Perpendicular Velocity Components

Rahul Sharma, Gary Verth, and Robertus Erdélyi
Solar Physics & Space Plasma Research Centre, University of Sheffield, Hicks Building, Hounsfield Road, Sheffield S3 7RH, UK
Received 2016 December 21; revised 2017 April 9; accepted 2017 April 10; published 2017 May 12

Abstract

Understanding the dynamic behavior of spicules, e.g., in terms of magnetohydrodynamic (MHD) wave mode(s), is key to unveiling their role in energy and mass transfer from the photosphere to corona. The transverse, torsional, and field-aligned motions of spicules have previously been observed in imaging spectroscopy and analyzed separately for embedded wave-mode identification. Similarities in the Doppler signatures of spicular structures for both kink and torsional Alfvén wave modes have led to the misinterpretation of the dominant wave mode in these structures and is a subject of debate. Here, we aim to combine line- of-sight (LOS) and plane-of-sky (POS) velocity components using the high spatial/temporal resolution Hα imaging-spectroscopy data from the CRisp Imaging SpectroPolarimeter based at the Swedish Solar Telescope to achieve better insight into the underlying nature of these motions as a whole. The resultant three-dimensional velocity vectors and the other derived quantities (e.g., magnetic pressure perturbations) are used to identify the MHD wave mode(s) responsible for the observed spicule motion. We find a number of independent examples where the bulk transverse motion of the spicule is dominant either in the POS or along the LOS. It is shown that the counterstreaming action of the displaced external plasma due to spicular bulk transverse motion has a similar Doppler profile to that of the $m = 0$ torsional Alfvén wave when this motion is predominantly perpendicular to the LOS. Furthermore, the inferred magnetic pressure perturbations support the kink wave interpretation of observed spicular bulk transverse motion rather than any purely incompressible MHD wave mode, e.g., the $m = 0$ torsional Alfvén wave.

Key words: magnetohydrodynamics (MHD) – Sun: chromosphere – Sun: oscillations

1. Introduction

One of the major problems in solar physics today is identifying the energy transfer mechanisms throughout the chromosphere and transition region. A key observational "window" into this problem is the study of spicules, which are thin, long, jet-like magnetic features that populate the highly dynamic and complex region between the solar photosphere and corona. These enigmatic structures are observed in chromospheric spectral lines such as Hα, Ca II H and K, and He I D3 from both ground- and space-based instrumentation and are a focus of wave physics in the solar chromosphere (Zaqarashvili & Erdélyi 2009; Jess et al. 2015; Verth & Jess 2016). Ever since their discovery by Secchi in 1877, spicules have been the topic of much debate in the solar physics community. Understanding spicules has been hampered by instrumental limitations, and their high velocities, short visible lifetimes, and narrow widths. Also, spectral diagnostics off-limb, where spicules are easier to identify, are further complicated by the presence of many superimposed structures in the line of sight (LOS). This makes it challenging to decipher the true motions of spicules and to identify the possible presence of magnetohydrodynamic (MHD) wave modes.

Spicules are often modeled as thin magnetic flux tubes since their widths are far less than their heights. As a further approximation, spicules are modeled as axisymmetric cylindrical waveguides that bridge the lower and upper solar atmospheres. MHD waves passing through these structures can be classified using azimuthal (m) and axial (k_z) wave numbers, derived from observable quantities (frequency, phase speed, wavelength). In theory, spicules may support a superposition of MHD waves of any azimuthal wave number m. However, thus far there have only been claims of identifying very low order m modes from spicule observations such as the $m = 0$ torsional Alfvén wave (De Pontieu et al. 2012) and the $m = 1$ kink wave (Kukhianidze et al. 2006). The estimated phase/group speeds can further indicate the corresponding surface/body modes for a given theoretical equilibrium model. Interestingly, in the linear regime, magnetic tension is the only restoring force for the incompressible torsional Alfvén wave and is the main restoring force for the weakly compressible kink wave. Hence, analysis of two-dimensional (2D) imaging-spectroscopy data can give somewhat similar signatures for both Alfvén and kink waves. The difficulties of interpretation have been discussed by, e.g., Erdélyi & Fedun (2007), Erdélyi & Taroyan (2008), Van Doorsselaere et al. (2008), Zaqarashvili & Erdélyi (2009), and Mathioudakis et al. (2013). Accurate identification of wave modes is crucial in estimating their energy flux and damping mechanism/rate.

Spicule dynamics, reported in previous observational studies, are broadly classified into three separate domains: field-aligned flows, transverse motions in the plane of sky (POS) detected via imaging, and torsional motions identified in Doppler shifts along the LOS. The transverse and torsional motions are often interpreted as kink and Alfvén waves, respectively. Kukhianidze et al. (2006) reported the first kink mode observations in spicule structures from spectroscopy data in their excellent but perhaps unfairly less recognized paper. They advocated that the oscillatory phenomenon observed in spicules is mainly due to kink waves excited by buffeting motion due to photospheric granulation. Transverse motion in spicules with amplitudes of the order of 10–12 km s^{-1} and periodicities of 100–500 s were observed by De Pontieu et al. (2007) and interpreted by these authors as "Alfvénic" waves. This label has become the subject of much controversy since that particular interpretation rested on the assumption of a homogeneous plasma in planar geometry,

whereas the chromosphere is actually finely structured and highly inhomogeneous. Later, a mix of upward, downward, and standing "Alfvénic" transverse waves along spicules were identified by Okamoto & De Pontieu (2011). Ebadi & Ghiassi (2014) analyzed high-cadence Ca II H data from *Hinode*/SOT and found upward propagating kink waves and their reconnection-like origins, while Tavabi et al. (2015) analyzed data for polar spicules and also found signatures of transverse waves. More significant transverse velocities of up to 60 km s^{-1} were reported by Pereira et al. (2012), which resulted in spicule axis displacements of up to 1 Mm, along with upward flows of the order of 100 km s^{-1}.

De Pontieu et al. (2012) claimed to have observed spicule rotational motions in Doppler measurements of the order of 25–30 km s^{-1} and inferred the presence of $m = 0$ torsional Alfvén waves. This interpretation was challenged by Goossens et al. (2014), who demonstrated that Doppler signatures for $m = 0$ torsional Alfvén wave can actually resemble those generated by $m = 1$ kink waves if the LOS is approximately perpendicular to the bulk transverse motion. Sekse et al. (2013) carried out similar observations for on-disk spicules and further confirmed their rotational motions and transverse displacements.

In this paper, the identification and interpretation of observed MHD wave mode(s) are presented along with estimates of magnetic pressure perturbations for observed spicules. For the first time, three-dimensional (3D) velocity vector reconstructions are derived for spicules by combining LOS Doppler velocity with POS transverse velocity components. Furthermore, we estimate the time- and space- dependent LOS magnetic field component, which provides insight into the magnetic pressure changes due to spicule dynamics.

2. Observations

The instrument used was the CRisp Imaging Spectro-Polarimeter (CRISP) at the Swedish 1-m Solar Telescope (Scharmer et al.2003, 2008) on La Palma. The Hα imaging-spectroscopic data of 07:15–07:48 UT, 2012 June 21, is of Active Region NOAA AR11504, which consisted of two sunspots at limb position (heliocentric coordinates with respect to disk center, hereby denoted by $\Theta = 893$, $\Phi = -250$). The AR was scanned using 31 equally spaced line positions with 86 mÅ, steps from -1.376 to $+1.29$ Å, relative to line center, along with four additional positions in the far blue wing from -1.376 to -2.064 Å. These data were then further processed using the Multi-Object Multi Frame Blind Deconvolution (MOMFBD; van Noort et al. 2005) image restoration algorithm. Also, standard procedures available in the image pipeline for CRISP data (de la Cruz Rodríguez et al. 2015), including differential stretching and removal of dark- and flat-fielding, were implemented. The final science-grade data of ~30 minute duration had a pixel size of 0.″059 (~43 km) with a cadence of 7.7 s.

The resultant data shows spicule structures (Figure 1) at far-wing positions in the Hα line profile. Spicules appear in clusters or bushes, which makes identification and tracking of individual structures a challenging task. Eight spicule structures were finally selected for this study, on the basis that they were distinct enough from the background and other features in the image frame during their lifetime in the respective line-scan positions. The observed lifetimes, inclination, and velocity ranges in both POS and LOS domains are given in Table 1 and were found consistent with previous reports (Tsiropoula et al. 2012). The average lifetime of the spicules under study was found to be around 127 s while the inclination angle with respect to the vertical is about 25°.47. Subsequent space- and ground-based, full-disk images from earlier dates support the fact that the observed off-limb spicules originated from a quiet-Sun region, nearly along the same projected LOS as the observed active region, although this could not be validated from the data used in the present study.

Figure 2 shows a cartoon of a spicule whose LOS integrated intensity is projected onto a 2D image plane. The observed spicule extends from the upper photosphere to the lower corona and its inclination angle relative to the plane of the photosphere can influence the observed brightness, apparent height, and Doppler velocity (Athay & Bessey 1964).

3. Methods

The x- and z-components of the velocity vectors in the POS were estimated using the Fourier Local Correlation Tracking algorithm (FLCT; Fisher & Welsch 2008). This technique is based on the cross-correlation of intensity features observed in successive frames to estimate POS motions. The main assumption for this technique is that any variation in the pixel intensity value is entirely due to plasma motion and not because of thermal changes. Three input parameters are required for the FLCT algorithm to estimate velocity. A sigma value specifies the size of the window for the correlation function, a minimum intensity threshold, and a function "K" which serves as a low-pass filter to reduce high-frequency noise. Input parameters for the FLCT routine were tested rigorously by introducing an artificial shift in the test images and determining the most probable parameters that match the shift. Also, time–distance analysis for the spicule structures at different heights provided estimates for possible displacement changes in time. FLCT parameters were updated for these changes to derive the most optimal velocity outputs for the observed features. Although there are no direct methods to estimate the errors associated with these velocity measurements, for the interested reader, the uncertainties associated with the input region of interest (ROI) for the FLCT algorithm are discussed in detail in the appendix to Freed et al. (2016).

Spectroscopic measurements in the Hα spectral line at 35 line positions were used to estimate the LOS velocity component. The Doppler velocity estimation for spicules is not straightforward. Each image frame with the ROI has pixels with both absorption and emission profiles (Figure 3). This results in the selected spicules having asymmetric line profiles, restricting the use of simple fitting procedures. To address this, we employed a double-Gaussian function given by

$$I(\lambda) = b + I_1 \exp\left\{\frac{(\lambda - \mu_1)^2}{2\sigma_1^2}\right\} + I_2 \exp\left\{\frac{(\lambda - \mu_2)^2}{2\sigma_2^2}\right\},$$

where $I(\lambda)$ is the discrete intensity line profile, λ is the wavelength, b is the background signal level, I is the intensity, μ is the mean of the distribution, and σ is the standard deviation. The number in the subscript refers to the two Gaussians. Further, line profiles from spicules show multiple peaks. A potential explanation could be the LOS superposition effects from multiple threads in spicule structure (Skogsrud et al. 2014). A similar explanation was also postulated by Antolin et al. (2014), where they showed that

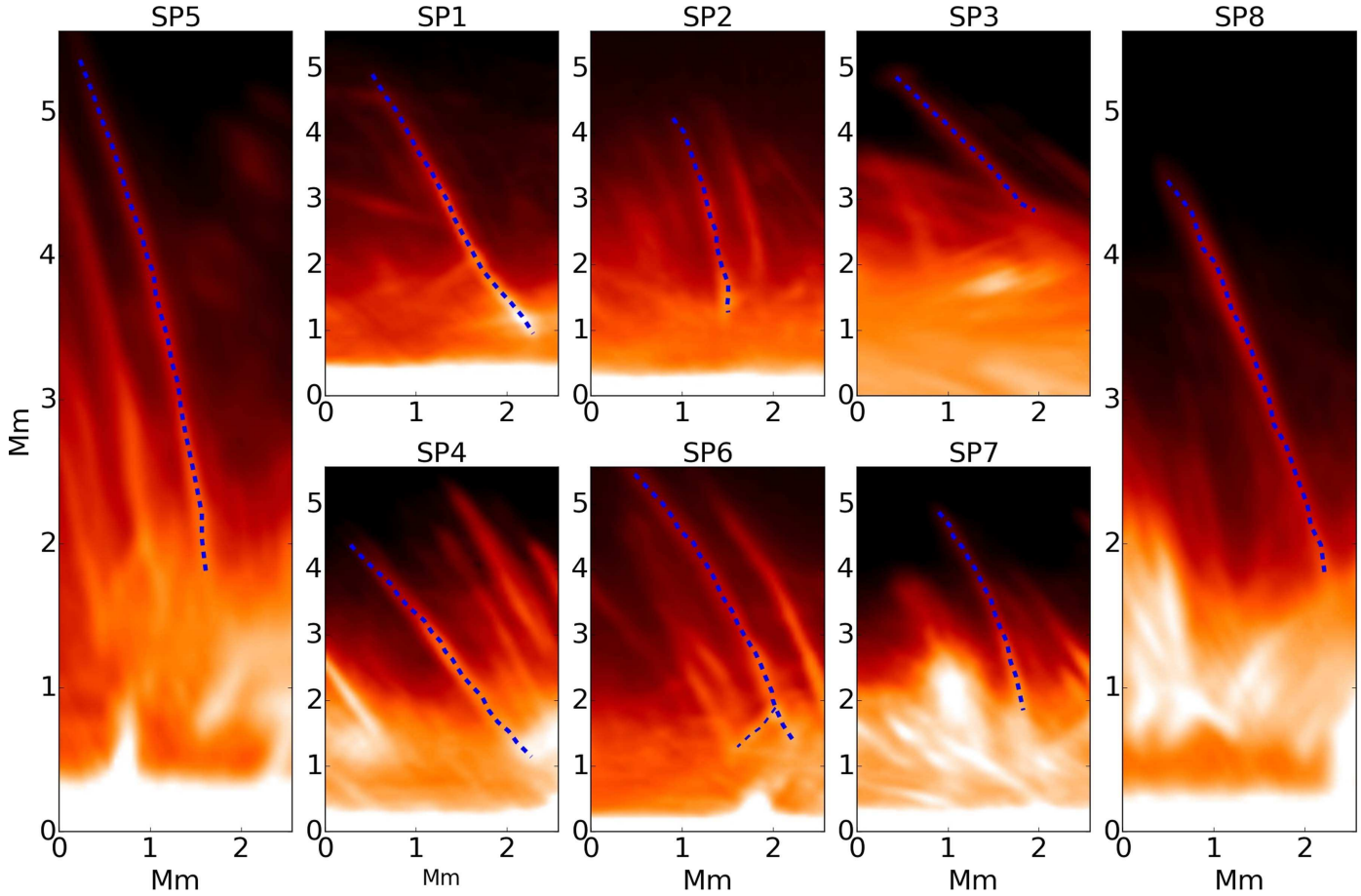

Figure 1. Examples of Hα limb spicules (marked by the dashed line) at different line-scan positions. The features were selected for the least possible superposition with any nearby structures during its lifetime in the observed line-scan positions. In this paper, two spicules are presented in detail as being representative examples of having their bulk transverse motion mostly in the POS (SP5) or along the LOS (SP8).

Table 1
Data of the Eight Spicules Studied Including POS and LOS Velocity Range and the Dominant Plane of Transverse Motion

Spicule	λ_s (Å)	T_i (minute)	$T_{\rm tot}$ (s)	Length (Mm)	Height (Mm)	Inc. Angle (°)	$\rm POS_{vel}$ (km $\rm s^{-1}$)	$\rm LOS_{vel}$ (km $\rm s^{-1}$)	$\rm Plane_{trans}$
SP1	−1.204	5.9	100.1	4.1	4.9	23.6	−11.6–16.7	−37.1–25.0	LOS
SP2	−1.209	19.5	84.7	2.5	4.1	13.0	−5.6–11.1	−13.5–24.1	LOS
SP3	+0.430	21.8	92.4	2.2	4.8	35.7	−16.7–16.7	−13.0–44.7	LOS
SP4	−1.032	21.9	61.6	3.7	4.4	32.2	−16.7–27.9	−8.8–1.8	POS
SP5	−1.032	21.6	215.6	3.8	5.3	21.4	−27.9–33.5	−12.0–10.0	POS
SP6	−1.118	22.3	123.2	3.8	5.4	24.5	−16.7–22.3	−8.2–12.4	POS
SP7	−1.204	33.5	84.7	2.5	4.4	20.2	−11.6–11.6	−22.9–29.5	LOS
SP8	−0.946	25.2	254	3.1	4.4	33.0	−5.6–11.6	−17.9–29.3	LOS

Note. λ_s is the line-scan position from the Hα line core, T_i is the time when the spicule first appeared in the observed line-scan position, while $T_{\rm tot}$ is the total lifetime of the spicule structure. The apparent visible length and apex height of the spicules under study are shown in the following columns. Inclination angle indicates the tilt of the spicules w.r.t. the vertical. Velocity ranges of spicular waveguides in both POS and LOS are given in subsequent columns with the dominant plane of transverse motion.

multiple thread-like features could be generated by a combination of the LOS angle and K-H vortices resulting from large amplitude transverse MHD wave propagation (Scullion et al. 2011).

The estimated LOS and POS with mean errors ± 4.34 km $\rm s^{-1}$ and ± 2.76 km $\rm s^{-1}$, respectively, are then combined to determine the 3D velocity vector at each pixel projected onto the 2D image plane. With time cadence (δt), the resultant 3D velocity vector ($\boldsymbol{v}_r$) can also provide the displacement ($\boldsymbol{v}_r\,\delta t$) and acceleration ($\delta \boldsymbol{v}_r/\delta t$) at each pixel, giving a more detailed insight into the time and space evolution of the plasma dynamics of spicules.

4. Results

In this section, spicule velocity vector maps, along with other quantities (resultant displacement, acceleration) will be constructed by combining LOS and POS velocity estimates at every pixel in the 2D image frame. Furthermore, particular examples of spicules with their transverse motion mostly in the LOS or POS will be examined in detail to identify the possible

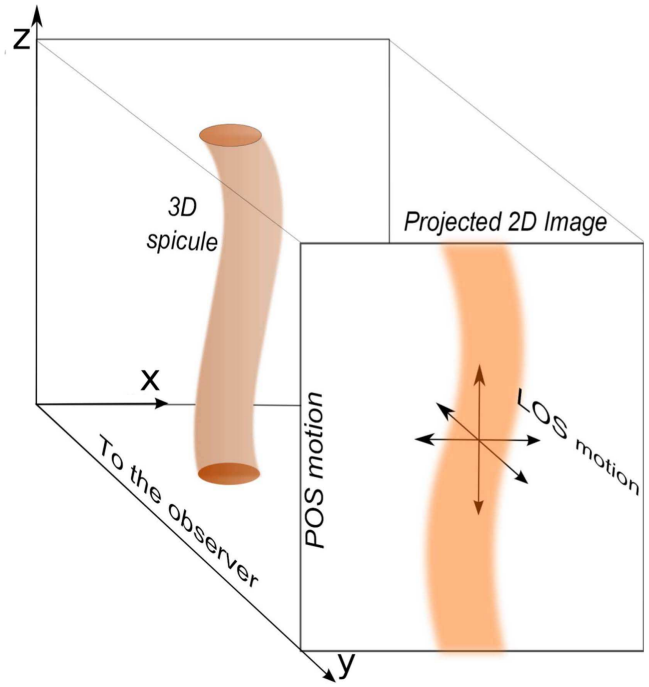

Figure 2. Cartoon showing the LOS intergrated spicule intensity projected onto a 2D image plane. Here, the spicule is projected onto the *xz*-plane with the *z*-axis normal to the surface and the *y*-axis along the observer's LOS. The actual 3D plasma velocity is a resultant of the estimated LOS and POS components at each pixel.

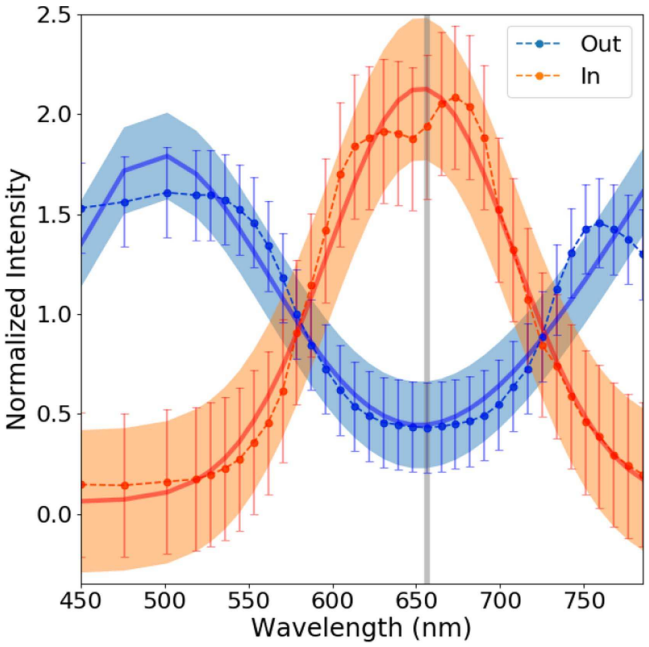

Figure 3. Examples of a double-Gaussian fit to the line profile of pixels, both inside and outside the spicule structure. The dotted–dashed line marks the normalized intensity magnitudes at the line-scan positions on either side of the line center (marked by the vertical line) with $\pm\sigma$ as error bars. The solid line is the double-Gaussian fit with the σ confidence level of the overall fit as the highlighted region for both line profiles.

presence of MHD wave modes through their velocity and associated magnetic field perturbations.

The line-scan positions, lifetimes, velocity range in both LOS and POS, and dominant planes of transverse motion of the eight spicules shown in Figure 1 are listed in Table 1. The

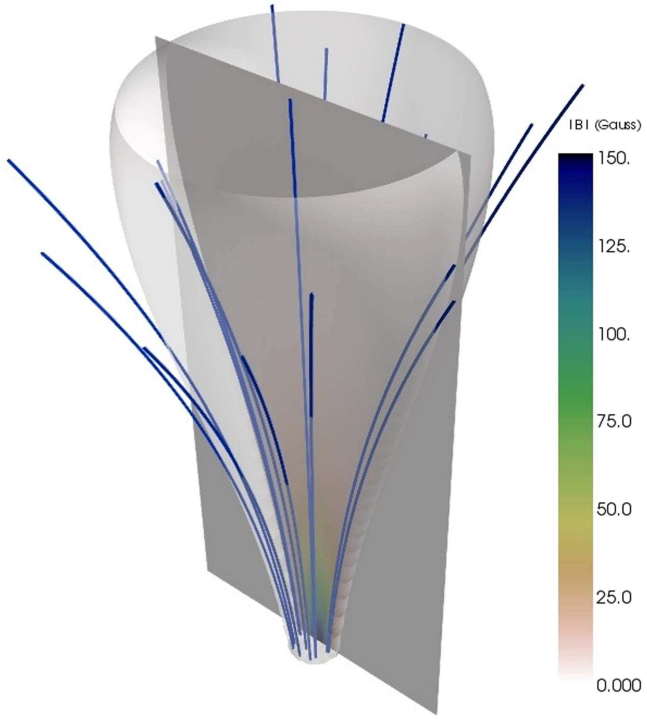

Figure 4. 3D rendering of the background magnetic field along with selected field lines. The isosurface illustrates the expanding intergranular magnetic field with an exponential drop in magnetic field strength with height. A vertical 2D slice of the background magnetic field is illustrated in the middle, which is used to estimate the associated model magnetic field perturbations from an observed spicule's velocity field.

velocity estimate ranges for transverse motions are consistent with the previously reported cases referred to in Section 1. In this particular sample, about 40% of the spicules have the POS as the dominant plane of transverse motion. The other 60% have their transverse motion mainly along the LOS.

As a spicule undergoes this bulk transverse motion, it is pushing into the external plasma, hence it is natural to expect that pressure perturbations will accompany this movement. Even linear kink wave predicts this, although it must be noted that it is the restoring force of magnetic tension that dominates over any plasma and magnetic pressure perturbations in this regime. However, to date, measurement of magnetic pressure changes associated with transverse spicule motion has not been possible due to instrumental limitations and other technical difficulties with direct methods (e.g., Zeeman splitting and gyroresonant emission). To circumvent this, we will simply introduce a model background magnetic field and estimate the perturbations of this assumed magnetic field due to the observed time and space evolution of a spicule's velocity field. The model background field chosen here (as shown in Figure 4) is self-similar and the external atmospheric parameters are from Vernazza et al. (1981). Conveniently, this class of magnetic field is given by a simple closed analytical expression. The full description of the methods employed to construct such a field, along with boundary conditions and tests, are given by, e.g., Shelyag et al. (2008) and Gent et al. (2013). It is known that intergranular magnetic fields are measured to be between 100 and 200 G for the quiet-Sun region (Trujillo Bueno et al. 2004); therefore, we choose the footpoint magnetic field to be 150 G.

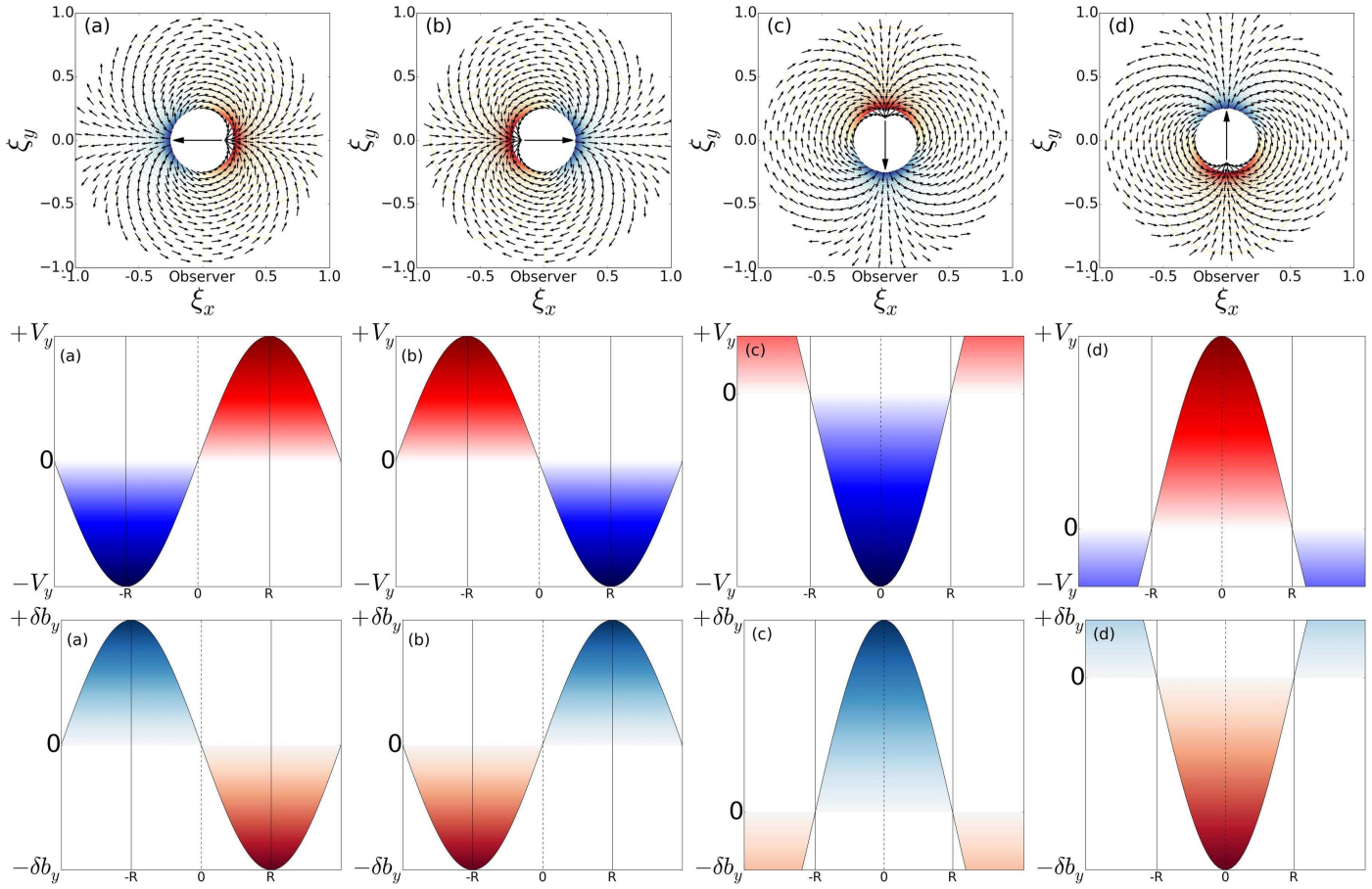

Figure 5. Spicule undergoing linear kink wave motion where the bulk transverse motion is perpendicular (panels (a) and (b)) and parallel (panels (c) and (d)) to the LOS. The plasma is assumed to be optically thick. The top row shows the spicule's displacement field (ξ) in the xy-plane with the observer's LOS along the y-axis. The arrow at the center of the spicule marks the direction of its motion and the perturbed magnetic pressure color-coded around its boundary. The corresponding profiles for the Doppler velocities (V_y) and the perturbed y-component of the magnetic field (δb_y) are given in panels below for the spicule with radius (R).

In order to have an estimate for the perturbations in magnetic pressure for the given background magnetic field, we employ 3D velocity vector components in the linearized induction equation. The velocity vectors, $\boldsymbol{v}(x, y, z, t)$, in terms of tube displacement, $\boldsymbol{\xi}(x, y, z, t)$, can be given as $\boldsymbol{v} = \delta\boldsymbol{\xi}/\delta t$. For the model chromospheric background magnetic field $\boldsymbol{B}_0$, the induction equation can be expressed as

$$\delta\boldsymbol{b} = \nabla \times (\delta\boldsymbol{\xi} \times \boldsymbol{B}_0). \tag{1}$$

Since $\delta\boldsymbol{\xi}_n = \boldsymbol{\xi}_n - \boldsymbol{\xi}_{n-1}$ is the change in displacement of the tube at a given frame number n, the perturbed magnetic field can be rewritten as

$$\delta\boldsymbol{b}_n = \nabla \times [(\boldsymbol{\xi}_n - \boldsymbol{\xi}_{n-1}) \times \boldsymbol{B}_0]. \tag{2}$$

The LOS component of the perturbed magnetic field is then

$$\delta b_{y,n} = \frac{\delta}{\delta x}(B_{0x}\delta\xi_{y,n} - \delta\xi_{x,n}B_{0y}) - \frac{\delta}{\delta z}(B_{0y}\delta\xi_{z,n} - \delta\xi_{y,n}B_{0z}). \tag{3}$$

Here, B_0 and $\delta\xi$ with subscripts x, y, z refer to the components of the background magnetic and estimated displacement fields. Equation (3) is applied in Sections 4.1 and 4.2 for two particular spicules, SP5 and SP8, to model LOS magnetic field perturbations with their observed velocity field dynamics as an input. Spicules SP5 and SP8 are discussed in detail since they are representative examples that have their transverse motion mostly in the POS or along the LOS.

To compare observations with linear kink wave theory, Figure 5 shows the Doppler shifts and magnetic pressure perturbations expected for an observer with an LOS both perpendicular and parallel to the bulk transverse motion (see, e.g., Goossens et al. 2014). Note that in Figure 5 the spicule plasma is taken to be optically thick, i.e., the emission on the observer side of the spicule is taken to be dominant. The comparison between the kink wave model and observation will be particularly insightful since the theory does not actually account for the fact that the spicule may not be in a quiescent environment.

4.1. Case 1. Transverse Motion Dominant in POS

Figure 6 shows an intensity image (I) of spicule SP5 observed at -1.032 Å, from the Hα line-core position and difference image (δI) with perturbed LOS Doppler velocity (δV_y), magnetic field (δb_y), and acceleration estimates. It can be seen that for the observed spicule the LOS Doppler velocity (Figure 6(c)) shows a red–blue Doppler shift asymmetry across its width, which has previously been interpreted as the signature of $m = 0$ torsional Alfvén waves by De Pontieu et al. (2012). Estimates for the acceleration (Figure 6(d)) show LOS magnitudes up to 1 km s^{-2} along the spicule. For our chosen background magnetic field, the magnitude of the LOS

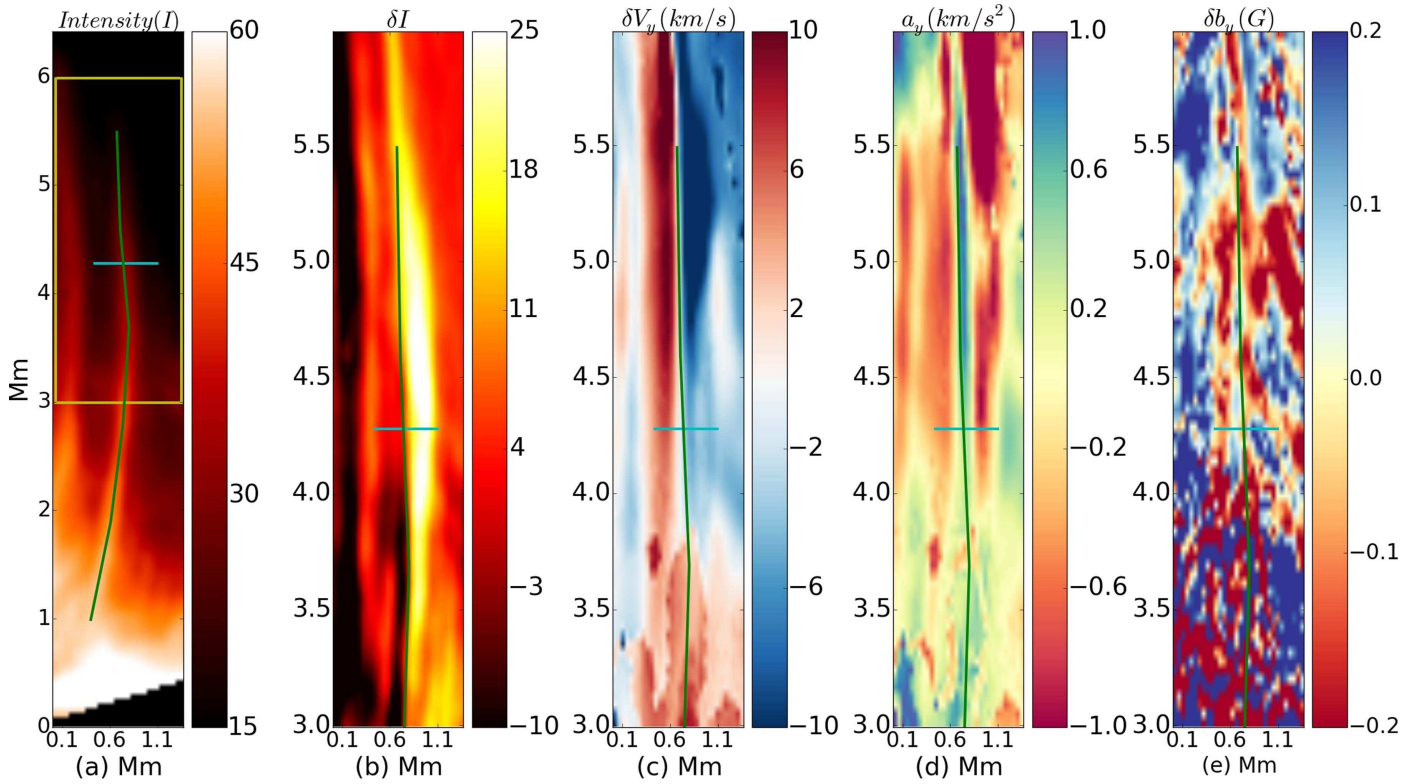

Figure 6. Observed and estimated parameters of spicule SP5 (marked by the line). In panel (a), the ROI is highlighted in the Hα intensity image. Panels (b) to (e) show the intensity difference (δI), Doppler velocity (δV_y), acceleration (a_y), and the LOS magnetic field perturbation (δb_y), respectively. The horizontal line marks the location of the slit used for the time–distance plot shown in Figure 7. Analysis of the intensity and Doppler shifts provided the POS and LOS velocity and acceleration components while the LOS magnetic field perturbation is used as a proxy for pressure changes in the vicinity of the spicule.

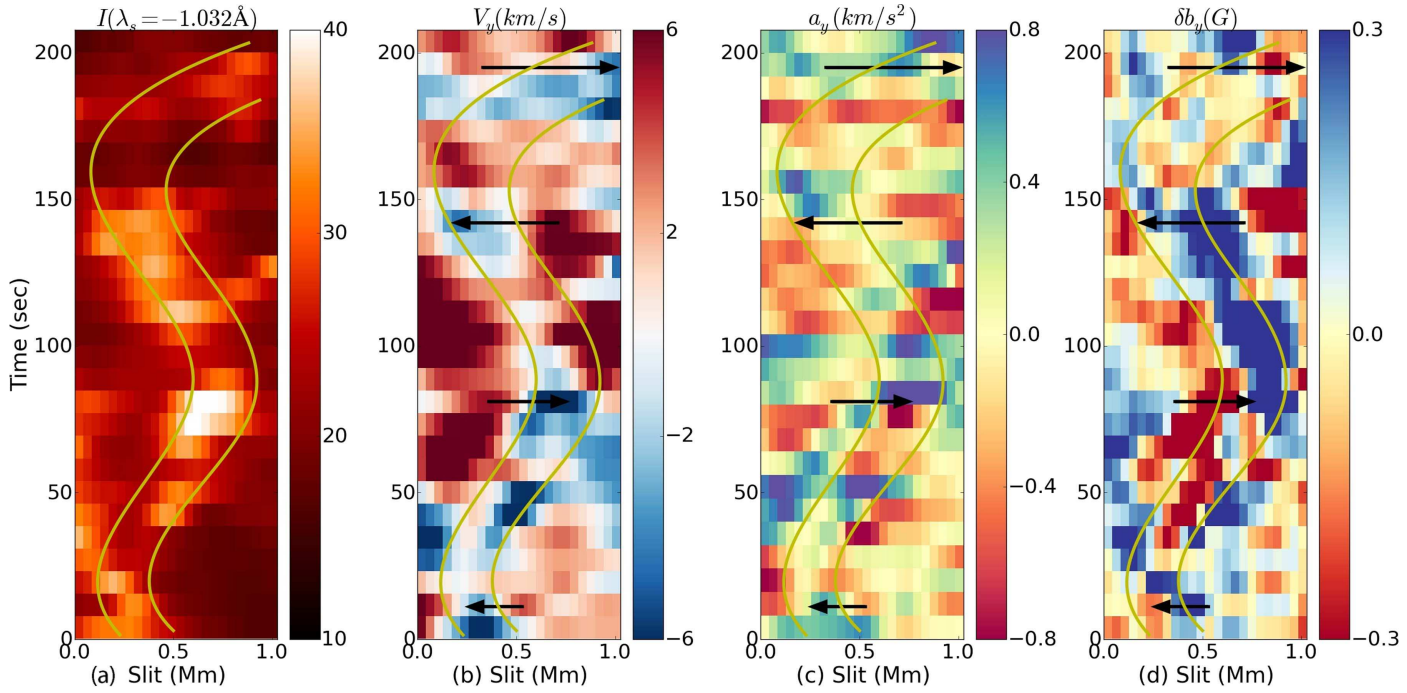

Figure 7. (a) Hα intensity (I) profile for spicule SP5 with its POS transverse displacement highlighted by the yellow lines. In panel (b), the positions of the arrows show that the Doppler velocity has a transverse red/blue asymmetry, which alternates with time. The arrows also mark the direction of spicule transverse displacement. In panels (c) and (d), at the arrow locations there is also evidence of transverse asymmetry in both acceleration and the perturbed LOS magnetic field.

perturbation shown in Figure 6(e) is up to 0.3 G. The magnitude of the perturbed magnetic field when compared to the background field is of the order of ∼0.01–0.13.

The POS displacement of spicule SP5 as a function of time can be seen in Figure 7. This indicates that there is a dominant component of the bulk transverse motion in the POS. At the

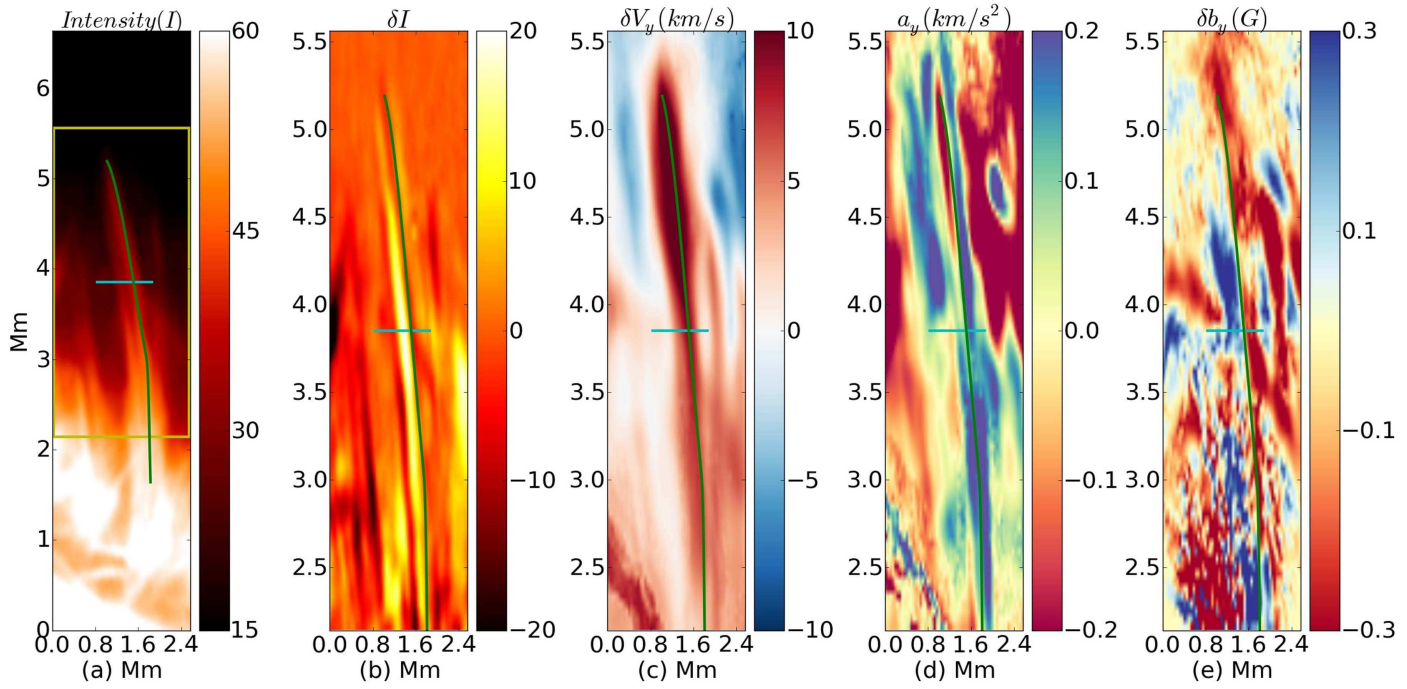

Figure 8. Observed and estimated parameters of spicule SP8 (marked by line). In panel (a), the ROI is highlighted in the Hα intensity image. Panels (b) to (e) show the intensity difference (δI), Doppler velocity (δV_y), acceleration (a_y), and the LOS magnetic field perturbation (δb_y), respectively. The horizontal line marks the location of the slit used for the time–distance plot shown in Figure 9.

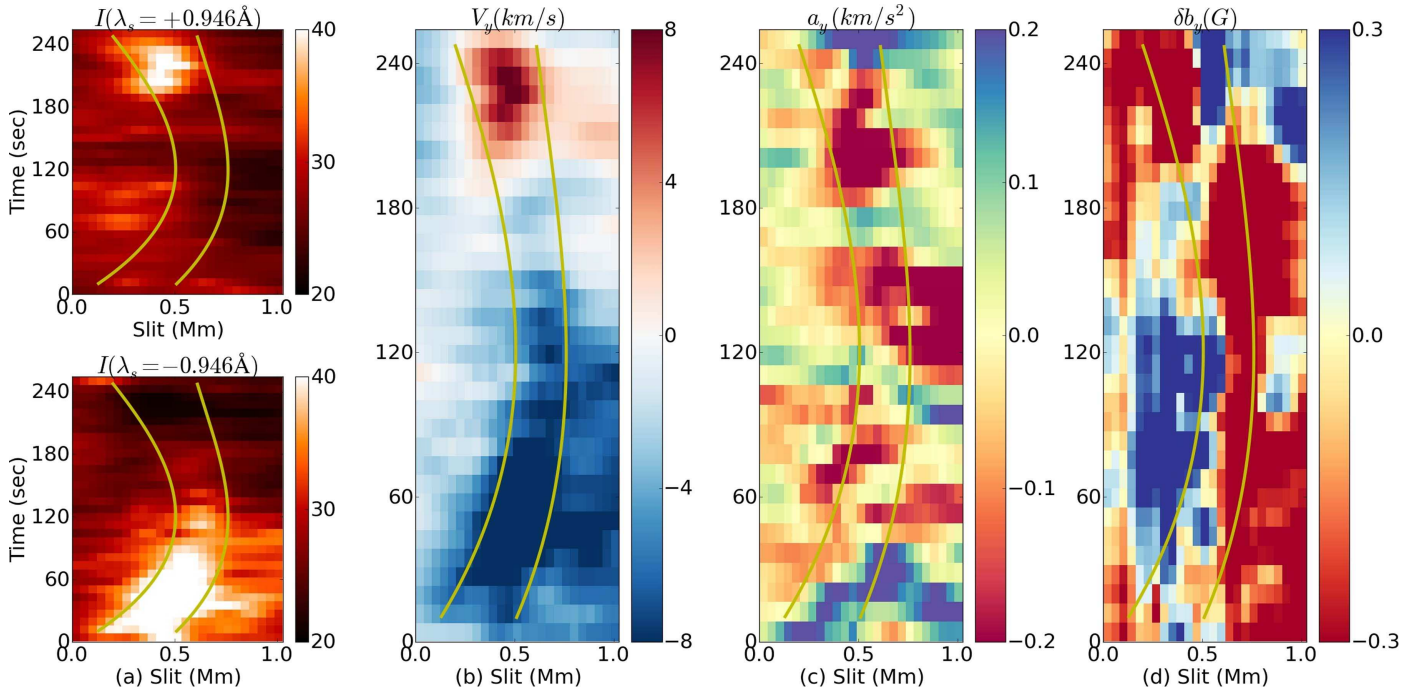

Figure 9. Comparison of timescale evolution of the observed/estimated parameters for spicule SP8. Panel (a) shows Hα intensity (I) profiles at line-scan positions ($\pm\lambda_s = 0.946$) and panel (b) shows Doppler shifts providing evidence that the bulk transverse motion of the spicule is along the LOS. Panels (c) and (d) show variations in acceleration (a_y) and the modeled LOS magnetic field perturbations (δb_y) along the spicule.

transverse anti-nodes, indicated by the black arrows, it can be seen in Figure 7(b) that the LOS velocity shows the same red–blue asymmetry across the spicule width as shown in Figure 6(c). The kink wave model shown in Figures 5(a) and (b) indicates that this asymmetry in Doppler velocity can be attributed to its associated $m = 1$ dipolar velocity field if the LOS is approximately perpendicular to the bulk transverse motion. This is an alternative explanation to the $m = 0$ torsional Alfvén wave interpretation of De Pontieu et al. (2012). Note also that the Doppler shifts are higher around the boundary of the spicule, indicating strong counterstreaming in the external plasma.

Although De Pontieu et al. (2007) interpreted the transverse waves observed in spicules with the Solar Optical Telescope on

board *Hinode* as being incompressible, Figure 7(d) shows that by inputting the estimated velocity field from both imaging and spectroscopy in Equation (3), a perturbed LOS component of the magnetic field is a natural consequence. Taking this as a proxy for magnetic pressure variations along the spicule, this questions the idea that these motions are incompressible. In fact, the kink wave model in Figures 5(a) and (b) predicts such asymmetric pressure variations across the width of the spicule if the LOS is approximately perpendicular to its bulk transverse motion. There is also supporting evidence of this asymmetry at the positions of the black arrows in Figure 7(d).

4.2. Case 2. Transverse Motion Dominant Along LOS

Figure 8 gives a comparison of the different observed and estimated quantities for spicule SP8. The slice across the spicule to produce the time–distance plots in Figure 9 is shown in Figure 8(a). It can be seen from Figures 8(c) and 9(b) that the Doppler velocity is symmetric across the width of the spicule. This is consistent with the kink wave model shown in Figures 5 (c) and (d), where the LOS is along the direction of the bulk transverse motion. This interpretation does not permit the appearance of an apparent $m = 0$ torsional Alfvén wave and is consistent with what we actually observe. If the LOS is perpendicular to the spicule axis, $m = 0$ motion is independent of the azimuthal viewing angle; however, $m = 1$ motion is not. From the data analyzed here, spicules that do not have a notable transverse POS motion do not exhibit the red–blue Doppler asymmetry across their widths, which De Pontieu et al. (2012) interpreted as $m = 0$ torsional Alfvén waves. Therefore, this supports the idea that the asymmetric Doppler shift across spicules shown in Figures 5(c) and 6(b) is actually due to $m = 1$ rather than $m = 0$ rotational motion. In such a scenario, the rotational and transverse motions could be coupled (see, e.g., Goossens et al. 2014) and this should be the focus of a future study.

The kink wave model of Figures 5(c) and (d) suggests that a positive Doppler velocity should correspond to a positive LOS magnetic field component. However, comparison between Figures 9(b) and (d) shows a more asymmetric profile for the modeled magnetic perturbation. Since the time–distance plots of Figure 9 also show a weaker but still noticeable transverse displacement in the POS, this could be due to external pressure gradients in the spicule's environment, or indeed another kink wave polarized at a different angle. The kink wave model illustrated in Figure 5 assumes that there is only one kink wave present and that the spicule is undergoing "free oscillation." Of course, this is highly idealized and the assumption of a quiescent environment may be far from reality. However, in agreement with Case 1 in Section 4.1, our modeling suggests that pressure forces in and around spicules play a part in their observed dynamics and that the initial interpretation of incompressible motion by De Pontieu et al. (2007) may have been too simplified.

5. Conclusions

To gain a better insight into the true nature of 3D spicular motion from observations, it is crucial to carefully analyze the LOS and POS velocity components and how they relate to each other. Here, we have achieved this by combining both imaging and spectroscopic Hα data from the high spatial temporal resolution CRISP instrument. From a case study of eight spicules, it was found that 40% had their bulk transverse motion mainly in the POS and the other 60% had this motion dominant along the LOS, with results consistent with those reported as Cases 1 and 2, respectively. This allowed us to analyze this transverse motion from two approximately perpendicular angles. When the LOS is mostly parallel to the transverse motion, no signatures of apparent $m = 0$ torsional Alfvén waves were found. However, when the LOS is almost perpendicular to the spicule transverse motion, a red–blue asymmetry, indicative of apparent $m = 0$ torsional Alfvén waves, is present. This contradiction can be most readily explained by the $m = 1$ kink wave, which has both transverse and rotational components that are *not* independent of the LOS. It should be the purpose of a future study to investigate possible coupling between these velocity components and whether mode conversion is taking place. Further support was found for the kink wave interpretation by modeling the LOS magnetic perturbation using estimates of the LOS and POS velocity as input for the magnetic induction equation. It was found that the spicular transverse motion cannot be assumed to be incompressible and that even pressure gradients in the environment may influence their observed dynamics. This investigation opens the way to obtaining more accurate information about actual 3D spicular motion. This knowledge is necessary for a more precise interpretation of MHD wave modes and estimation of their associated energy flux. The forthcoming DKIST instrument, with the highest spatial/temporal resolution yet, will provide another leap forward in this regard.

The Swedish 1-m Solar Telescope is operated by the Institute for Solar Physics of the Royal Swedish Academy of Sciences in the Spanish Observatorio del Roque de los Muchachos of the Instituto de Astrofisica de Canarias. R.E. was the PI of the observational campaign. The authors are grateful to B. Welsch, D. McKenzie, G. Fisher, and M. Freed for their insightful inputs regarding the FLCT algorithm and S. Shelyag for the background magnetic field model. We are also grateful to N. Freij and E. Scullion for their assistance in data acquisition. R.S. acknowledges support from the School of Mathematics and Statistics (SoMaS) for PhD studentship. R.E. acknowledges the support received by the Chinese Academy of Sciences President's International Fellowship Initiative, Grant No. 2016VMA045, the Science and Technology Facility Council (STFC), UK and the Royal Society (UK). This research has made use of SunPy, an open source and free community-developed solar data analysis package written in Python (SunPy Community et al. 2015).

References

Antolin, P., Yokoyama, T., & Van Doorsselaere, T. 2014, ApJL, 787, L22
Athay, R. G., & Bessey, R. J. 1964, ApJ, 140, 1174
de la Cruz Rodríguez, J., Löfdahl, M. G., Sütterlin, P., Hillberg, T., & Rouppe van der Voort, L. 2015, A&A, 573, A40
De Pontieu, B., Carlsson, M., Rouppe van der Voort, L. H. M., et al. 2012, ApJL, 752, L12
De Pontieu, B., McIntosh, S. W., Carlsson, M., et al. 2007, Sci, 318, 1574
Ebadi, H., & Ghiassi, M. 2014, Ap&SS, 353, 31
Erdélyi, R., & Fedun, V. 2007, Sci, 318, 1572
Erdélyi, R., & Taroyan, Y. 2008, A&A, 489, L49
Fisher, G. H., & Welsch, B. T. 2008, in ASP Conf. Ser. 383, Subsurface and Atmospheric Influences on Solar Activity, ed. R. Howe et al. (San Francisco, CA: ASP), 373
Freed, M. S., McKenzie, D. E., Longcope, D. W., & Wilburn, M. 2016, ApJ, 818, 57
Gent, F. A., Fedun, V., Mumford, S. J., & Erdélyi, R. 2013, MNRAS, 435, 689

Goossens, M., Soler, R., Terradas, J., Van Doorsselaere, T., & Verth, G. 2014, ApJ, 788, 9
Jess, D. B., Morton, R. J., Verth, G., et al. 2015, SSRv, 190, 103
Kukhianidze, V., Zaqarashvili, T. V., & Khutsishvili, E. 2006, A&A, 449, L35
Mathioudakis, M., Jess, D. B., & Erdélyi, R. 2013, SSRv, 175, 1
Okamoto, T. J., & De Pontieu, B. 2011, ApJL, 736, L24
Pereira, T. M. D., De Pontieu, B., & Carlsson, M. 2012, ApJ, 759, 18
Scharmer, G. B., Bjelksjo, K., Korhonen, T. K., Lindberg, B., & Petterson, B. 2003, Proc. SPIE, 4853, 341
Scharmer, G. B., Narayan, G., Hillberg, T., et al. 2008, ApJL, 689, L69
Scullion, E., Erdélyi, R., Fedun, V., & Doyle, J. G. 2011, ApJ, 743, 14
Sekse, D. H., Rouppe van der Voort, L., De Pontieu, B., & Scullion, E. 2013, ApJ, 769, 44
Shelyag, S., Fedun, V., & Erdélyi, R. 2008, A&A, 486, 655
Skogsrud, H., Rouppe van der Voort, L., & De Pontieu, B. 2014, ApJL, 795, L23
SunPy Community, Mumford, S., Christe, S. J., et al. 2015, CS&D, 8, 014009
Tavabi, E., Koutchmy, S., Ajabshirizadeh, A., Ahangarzadeh Maralani, A. R., & Zeighami, S. 2015, A&A, 573, A4
Trujillo Bueno, J., Shchukina, N., & Asensio Ramos, A. 2004, Natur, 430, 326
Tsiropoula, G., Tziotziou, K., Kontogiannis, I., et al. 2012, SSRv, 169, 181
Van Doorsselaere, T., Nakariakov, V. M., & Verwichte, E. 2008, ApJL, 676, L73
van Noort, M., Rouppe van der Voort, L., & Löfdahl, M. G. 2005, SoPh, 228, 191
Vernazza, J. E., Avrett, E. H., & Loeser, R. 1981, ApJS, 45, 635
Verth, G., & Jess, D. B. 2016, GMS, 216, 431
Zaqarashvili, T. V., & Erdélyi, R. 2009, SSRv, 149, 355